HHS Public Access

Author manuscript

Respir Physiol Neurobiol. Author manuscript; available in PMC 2021 June 01.

Published in final edited form as:

Respir Physiol Neurobiol. 2020 June ; 277: 103401. doi:10.1016/j.resp.2020.103401.

Endogenous glutamatergic inputs to the Parabrachial Nucleus/ Kölliker-Fuse Complex determine respiratory rate

Angela A. Navarrete-Opazo[a], **Denise R. Cook-Snyder**[b], **Justin R. Miller**[c], **Jennifer J. Callison**[a], **Nicole McCarthy**[b], **Barbara Palkovic**[a], **Eckehard A. E. Stuth**[a,e], **Edward J. Zuperku**[a,d], **Astrid G. Stucke**[a,e]

[a]Department of Anesthesiology, Medical College of Wisconsin, Milwaukee, Wisconsin

[b]Department of Neuroscience, Carthage College, Kenosha, Wisconsin

[c]Department of Biology, Carthage College, Kenosha, Wisconsin

[d]Zablocki VA Medical Center, Milwaukee, Wisconsin

[e]Children's Hospital of Wisconsin, Milwaukee, Wisconsin

Abstract

The Kölliker-Fuse Nucleus (KF) has been widely investigated for its contribution to "inspiratory off-switch" while more recent studies showed that activation of the Parabrachial Nucleus (PBN) shortened expiratory duration. This study used an adult, *in vivo*, decerebrate rabbit model to delineate the contribution of each site to inspiratory and expiratory duration through sequential block of glutamatergic excitation with the receptor antagonists 2,3-dihydroxy-6-nitro-7-sulfamoyl-benzo[f]quinoxaline-2,3-dione (NBQX) and d(−)-2-amino-5-phosphonopentanoic acid (AP5). Glutamatergic disfacilitation caused large increases in inspiratory and expiratory duration and minor decrease in peak phrenic activity (PPA). Hypoxia only partially reversed respiratory rate depression but PPA was increased to >200% of control. The contribution of PBN activity to inspiratory and expiratory duration was equal while block of the KF affected inspiratory duration more than expiratory. We conclude that in the *in vivo* preparation respiratory rate greatly depends on PBN/KF activity, which contributes to the "inspiratory on-" and "off-switch", but is of minor importance for the magnitude of phrenic motor output.

1. Introduction

Until recently, models of the respiratory rhythm generator focused on the preBötzinger Complex (preBötC) as the location of respiratory rhythm generation and on preBötC mechanisms to determine respiratory rate and pattern (Del Negro 2018; Molkov 2017). Models suggest that rhythm generation depends on the intrinsic bursting properties of pre-

Corresponding author: Astrid G. Stucke, M.D., Department of Anesthesiology, Medical College of Wisconsin, 8700 W Watertown Plank Road, Milwaukee, WI, 53201, Phone: 414-266-3560, Fax: 414-266-6092, astucke@mcw.edu.

inspiratory (pre-I) neurons that together with inspiratory (I) neurons generate an "inexorable" inspiratory burst (Kam et al. 2013; Del Negro 2018), which can be shortened by inhibition from post-inspiratory (post-I) neurons (Cui 2016). An alternative model holds that respiratory rhythm consists of three phases and is generated through reciprocal inhibition between "intrinsically rhythmogenic" pre-I/I neurons (Molkov 2017), post-I/ expiratory decrementing (E-dec) neurons (Ezure 1990) and augmenting expiratory neurons (Molkov 2017). In both models, the neurons of the medullary rhythm generator require tonic excitatory drive for regular discharge (Molkov 2017; Butera, Rinzel, and Smith 1999a). This drive is generally assumed to result from glutamatergic projections from the chemosensitive retrotrapezoid nucleus (RTN)(Bochorishvili 2012) as well as the pons (Geerling 2017), both of which have been defined in histological studies. Blockade of glutamatergic inputs to the preBötC results in loss of respiratory rhythm *in vivo* (Mutolo et al. 2005; Cook-Snyder 2019), and *in vitro* (Morgado-Valle and Feldman 2007).

The contribution of the pontine Kölliker-Fuse Nucleus (KF) to an "inspiratory off-switch" mechanism (Dutschmann et al. 2008) has been described in multiple studies where GABAergic inhibition (Dutschmann 2006), block of glutamatergic inputs to (Ling 1994) or lesioning (Feldman and Gautier 1976) of the area increased inspiratory duration. However, a specific excitatory "drive" from the KF to post- inspiratory neurons was only recently added to a model of the respiratory rhythm generator (Barnett 2018). Research has generally focused on the KF despite early publications that included the medial parabrachial nucleus (PBN) in this effect (Feldman and Gautier 1976). Our laboratory has repeatedly shown that alterations in PBN activity have a significant effect on expiratory phase duration (Zuperku 2019, 2017; Miller et al. 2017; Prkic et al. 2012). In the *in vivo* rabbit (Miller et al. 2017) and *in vivo* dog preparation (Prkic et al. 2012), excitation of the PBN through microinjection of glutamate agonists decreased expiratory duration while inhibition of the PBN through microinjection of opioids increased expiratory duration, suggesting the existence of excitatory inputs from the PBN to the "inspiratory on-switch" mechanism in the medullary rhythm generator. This was confirmed when Zuperku et al. showed that glutamatergic stimulation of the PBN resulted in increased activity in individual, extracellularly recorded pre-I neurons in the preBötC, which was associated with an increase in respiratory rate (Zuperku et al. 2017). Electrical stimulation of the PBN also resulted in increased excitatory inputs to other types of inspiratory neurons as well as E-dec neurons, i.e., neurons contributing to the "inspiratory on-" as well as "off-switch" (Zuperku 2019). To our knowledge, no study has compared the relative contribution of PBN versus KF activity to respiratory phase duration.

The purpose of the present study was to determine the contribution of PBN and KF activity to inspiratory and expiratory duration as well as the maximal effect of the entire pontine respiratory group, i.e., both PBN and KF, on respiratory phase timing. The PBN and KF can be functionally identified by typical changes in respiratory rate in response to local glutamate agonist injection: Tachypnea after α-amino-3-hydroxy-5-methyl-4-isoxazolepropionic acid (AMPA) injection has been used to identify the PBN (Prkic et al. 2012; Miller et al. 2017), while electrical stimulation (Dutschmann and Herbert 1998; Chamberlin and Saper 1992) or glutamate injection into the KF caused bradypnea (Levitt 2015; Dutschmann et al. 2008; Chamberlin and Saper 1994). Specifically, our goals were 1)

to establish the spatial relationship of the PBN (tachypnea) and KF (bradypnea) using functional identification with grid-wise AMPA injections; 2) to determine site specific contributions of the PBN and KF to inspiratory and expiratory phase duration with sequential local glutamate antagonist microinjection; 3) to examine whether very high levels of chemodrive, i.e., hypoxic hypercapnia, reversed respiratory rate slowing after glutamatergic block of the PBN/KF complex.

2. Materials and Methods

2.1. Surgical Procedures

This research was approved by the subcommittee on animal studies of the Zablocki Veterans Affairs Medical Center, Milwaukee, Wisconsin, in accordance with provisions of the Animal Welfare Act, the Public Health Service Guide for the Care and Use of Laboratory Animals, and Veterans Affairs policy. Experiments were carried out on adult (3–4 kg) New Zealand White rabbits of either sex. Animals were induced with 5 vol% sevoflurane via facemask and ventilated via tracheotomy with an anesthesia machine (Ohmeda CD, GE, Datex Ohmeda, Madison, WI). Anesthesia was maintained with 1.5–3% isoflurane. Inspiratory oxygen fraction, expiratory carbon dioxide concentration and expiratory isoflurane concentration were continuously displayed with an infrared analyzer (POET II, Criticare Systems, Waukesha, WI). Skin was infiltrated with lidocaine 1% before each skin incision. Femoral arterial and venous lines were used for blood pressure monitoring and infusion of solutions, respectively. Care was taken to increase anesthetic depth for any signs of “light anesthesia”, e.g., an increase in blood pressure or lacrimation. Lactated Ringer’s solution with 4 mcg/ml epinephrine was continuously infused at 1 ml/h. At this rate, the infusion did not result in appreciable changes in heart rate and blood pressure from baseline. Infusion rate was increased as needed to counteract or prevent hypotension in response to drug injections and/or from blood loss. The animal was maintained at 37.0 ± 0.5°C with a warming blanket. The animal was placed in a stereotaxic frame (David Kopf Instruments, Tujunga, CA), and blunt precollicular decerebration with complete removal of the forebrain was performed through a parietal craniotomy. After decerebration, isoflurane was either discontinued or continued at subanesthetic levels (0.3–0.4 vol%) for blood pressure control. Isoflurane concentration was not changed during the experimental protocol. The brainstem was exposed via occipital craniotomy and partial removal of the cerebellum. Animals were paralyzed with rocuronium (initially 1 mg/kg and redosed as needed) to avoid motion artifacts during neural/neuronal recording. Bilateral vagotomy was performed to achieve peripheral deafferentation to avoid interference of the mechanical ventilation with the underlying central respiratory rhythm and respiratory neuronal activity. The phrenic nerve and in some experiments the vagus nerve were recorded with fine bipolar electrodes through a posterior neck incision. Throughout the experiment animals were ventilated with a hyperoxic gas mixture (FiO_2 0.6) to achieve functional denervation of the peripheral chemoreceptors and at mild hypercapnia (expiratory carbon dioxide: 45–55 mmHg) to ensure sufficient respiratory drive (i.e., to keep baseline phrenic activity stably above the apneic threshold). Blood pressure was maintained stable throughout the protocols by adjusting the intravenous infusion rate. At the end of the experiment, animals were

euthanized with intravenous potassium chloride and the brainstem was removed and fixed for histological analysis.

2.2 Neuronal Recording, microinjection procedures and measured variables

All neuronal recording and microinjection techniques have been well established by our research group and have been previously described in detail (Dogas et al. 1998; Krolo et al. 1999). In short, extracellular neuronal recordings were obtained using multibarrel micropipettes (20–40 μm tip diameter) consisting of three drug barrels and a recording barrel containing a 7 μm thick carbon filament. Barrels were filled with the glutamatergic agonist, α-amino-3-hydroxy-5-methyl-4-isoxazolepropionic acid (AMPA, 50 μM, 70 nl/ injection), the NMDA receptor antagonist d(−)-2-amino-5-phosphonopentanoic acid (D-AP5; 5 mM, 700 nl/ injection) and the non-NMDA receptor antagonist 2,3-dihydroxy-6-nitro-7-sulfamoyl-benzo[f]quinoxaline-2,3-dione (NBQX; 1 mM, 700nl/ injection), which were dissolved in artificial cerebrospinal fluid. The microinjected volume was determined via height changes in the meniscus in the respective pipette barrel with a 100x monocular microscope and calibrated reticule (resolution ~3.5 nl). Respiratory neuronal discharge was recorded extracellularly from neuronal aggregates and individual neurons and classified by the temporal relationships relative to the phrenic neurogram. The neuronal and phrenic neural activity and pressure microejection marker signals were recorded using a digital acquisition system. These variables were also continuously displayed and recorded along with the phrenic neurogram, inspiratory time, expiratory time, discharge rate-meter, arterial blood pressure, airway carbon dioxide concentration on a computerized chart recorder (Powerlab/16SP; ADInstruments, Castle Hill, Australia). Before and after drug injection, steady-state conditions were obtained for respiratory parameters. Post experiment LabChart data was exported to SigmaPlot 11 (Systat Software, San Jose, CA) for data reduction, data plotting and statistical analysis. Between 10 and 50 consecutive respiratory cycles were averaged over 1–2 min with the number of cycles dependent on the respiratory rate. Using the phrenic neurogram we determined peak phrenic activity (PPA), respiratory rate (RR) and inspiratory (TI) and expiratory (TE) duration. Since changes in PPA closely reflect changes in respiratory tidal volume but the absolute value does not correspond with the absolute tidal volume (Eldridge 1976), PPA was normalized to control values for all calculations.

2.3 Functional mapping of the pontine respiratory group with AMPA injection.

Identification of the PBN through the tachypneic response to AMPA injection has been described before (Prkic et al. 2012; Miller et al. 2017). Similarly, Levitt et al. and Dutschmann and Herbert described identifying the KF by the bradypneic response to glutamate (Levitt 2015; Dutschmann 2006) and commented that injection into an area more rostral and medial resulted in tachypnea. To improve our understanding of the spatial relationship between the two areas and to reliably identify the PBN and KF in the current and future studies we constructed a map of the pontine respiratory group based on the changes in phrenic respiratory rate and PPA with AMPA microinjections.

We inserted the microelectrode in a grid-wise fashion starting at the caudal end of the inferior collicle at 1.5mm lateral from midline and moved up to 2mm lateral and 5mm caudal, dependent on the respiratory rate response to AMPA injection. Step size was 0.5mm

medio-lateral and 0.47mm rostro-caudal (i.e., a 0.5mm step size corrected for a 20°- rostro-caudal angle between brainstem and stereotaxic frame). In areas where neuronal activity was encountered, we microinjected AMPA (50 μM, 70nl) starting at the ventral limit of the neuronal activity and then in 1 mm steps more dorsally until there was no neuronal activity detected or no more changes in the phrenic neurogram. If the maximal response was encountered at the most ventral coordinate, we typically advanced the electrode 1mm more ventral and repeated the AMPA injection. The maximal AMPA effect on respiratory rate and PPA occurred within 30 sec of the injection and, dependent on the location of the injection, could last ~2–8 minutes. Subsequent injections were only made after full recovery. Injections were not repeated at the same location as the injection protocol was already very lengthy. Bilateral identification of the areas where AMPA caused maximal tachypnea and bradypnea usually required between three and four hours. Baseline respiratory rate did not change much over the course of the AMPA injection protocol suggesting that the tissue and neuronal networks were not substantially altered by the multiple injections. The area of maximal AMPA-induced tachypnea was labeled “PBN” and the area of maximal bradypnea was labeled “KF”. After successfully mapping the areas of interest, the animals were used for further study protocols as described below.

2.4. Functional differentiation between the Parabrachial Nucleus and Kölliker-Fuse Nucleus area with AMPA injection

To better delineate the functional difference between the PBN and KF, we compared changes in respiratory rate with AMPA microinjection into adjacent PBN and KF. Both sides of the brainstem were analyzed independently. Data were used for injections performed at PCO2 40 mmHg.

After pilot experiments suggested that bradypnea with AMPA injection into the KF was difficult to observe at higher PCO2 levels we performed a separate sub-study that repeated AMPA microinjections into the same KF location at PCO2 40mmHg and PCO2 50mmHg. Animals whose data were used for analysis of AMPA effect were subsequently used for other study protocols.

2.5. Histology

After conclusion of all experimental protocols, bilateral microinjections (140 nl) of fluorescent latex microspheres (Lumafluor.com; Red Retrobeads), diluted to 5% of the supplied concentration, were used to mark the PBN (area of maximal tachypnea) and KF (area of maximal bradypnea) for histological analysis. After euthanasia the brainstem was removed and submersed in paraformaldehyde (4%) fixative for 5 days and then stored in hypertonic sucrose (30% in PBS) with sodium azide (0.1%) before being flash frozen in isopentane and sectioned using a cryostat (Leica). Sequential coronal sections (of 20 μm thickness) were cut from the caudal edge of the inferior colliculi to 2-mm caudal to obex. For immunolabeling, free-floating sections were incubated in blocking solution (0.1 M phosphate buffered saline, 5% normal donkey serum, and 0.25% Triton X-100) for 1 h at room temperature. Sections were incubated in blocking solution with primary antibody sheep anti-TH (1:500, Millipore, AB1542) for 24 h at 4°C. The immunohistochemical staining pattern obtained with the anti-TH antibody was in agreement with the known

expression patterns of the corresponding proteins, both at the cellular and subcellular level, supporting the specificity of these antibodies. Sections were incubated with donkey anti-sheep Alexa Fluor 647 (1:500) antibodies for 2 h at room temperature (Jackson ImmunoResearch). Sections were counterstained with NeuroTrace 435/455 Blue Fluorescent Nissl Stain (1:25, Invitrogen, N21479), then mounted to glass slides using Fluoromount-G (Southern Biotech), coverslipped, and stored at 4°C until imaging. A confocal laser-scanning microscope (Nikon C2+) at a 4x objective was used for all image acquisition. The settings for PMT, laser power, gain, and offset were identical between experimental groups. The atlas of Meessen and Olszewski was used for identification of relevant regions (Meessen 1949).

2.6. Inhibition of glutamatergic inputs to the Parabrachial Nucleus and Kölliker-Fuse Nucleus

The experimenters were not blinded to the experimental conditions for any of the protocols. This protocol established the changes in respiratory rhythm when endogenous glutamatergic excitation of the PBN and KF areas was blocked by microinjections of the non-NMDA antagonist NBQX (1 mM, 700nl) and the selective NMDA antagonist AP5 (5 mM, 700nl). To confirm that the glutamate antagonist effects were independent of the order of injection similar to previous studies in the medullary rhythm generator (Cook-Snyder 2019), we performed a pilot study in a separate set of animals where the order of the glutamatergic antagonists was reversed, i.e., where AP5 was injected first.

For all injection protocols, the PBN and KF were identified bilaterally with grid-wise AMPA microinjections as described above. In a first set of animals, NBQX was microinjected bilaterally into the PBN. After three minutes, when changes in respiratory parameters had reached steady state, AP5 was microinjected bilaterally at the same coordinates. After reaching steady-state (~3min), NBQX was microinjected bilaterally into the KF, and after three minutes AP5 was microinjected bilaterally into the KF. The timeline was chosen based on a pilot study where NBQX and AP5 were injected only into the PBN (n=12).

To determine whether the order in which the areas were injected altered the antagonist effect, in a second group of animals we performed the antagonist injections in the reverse order, i.e., first into the KF and then into the PBN. Only one complete sequential protocol was performed per animal.

Glutamate antagonist injections resulted in significant respiratory rate slowing (bradypnea). To test whether a hypoxic stimulus in addition to the continued hypercapnia could increase respiratory rate after glutamate antagonism in the pontine respiratory group, at the end of the experiment we switched ventilation to FiO2 0.17 for 1–2 minutes. Expiratory CO2 at that time was 49±2mmHg. We subsequently paused the ventilator for one minute to achieve severe hypoxia. This maneuver also increased expiratory CO2 to 65±4 mmHg.

2.7. Statistical Analysis

Post-hoc data reduction, data plotting and statistical analysis of the pooled data were performed using SigmaPlot 11 (Systat Software, Richmond, CA). Sample size was based on published *in vivo* studies using similar protocols (Cook-Snyder 2019; Stucke et al. 2015; Miller et al. 2017). Data sets were tested for normal distribution (Shapiro-Wilk test).

Statistical tests were performed on raw data except for peak phrenic activity (PPA), which is measured in arbitrary units and thus normalization to control is necessary to allow for comparison between animals.

The effects of sequential AMPA injection into the PBN and KF and of sequential NBQX and AP5 injections into the PBN and KF on all respiratory parameters were determined using two-way, repeated-measures analysis of variance (ANOVA) with factors: site and drug, with Holm-Sidak correction for multiple comparisons (3.2. and 3.4.). The effect of hypoxia was analyzed for a subgroup of the animals undergoing the NBQX/AP5 protocol. Respiratory parameters were compared for the states control, complete glutamate antagonism and hypoxia using one-way, repeated measures ANOVA with Holm-Sidak correction for multiple comparison (3.4.). The magnitude of changes in TI and TE with glutamate antagonist injection dependent on the order of injection (PBN vs. KF first) was compared with a Mann-Whitney U test for categorical data (control, first injection site, second injection site)(3.5.1.).

PBN and KF contributions to phase timing were estimated using a physical timer model where the sum of the inputs (Σ) determines the time (T) until the threshold (V_{thresh}) is reached and the phase is terminated, i.e., $T = V_{thresh} / \Sigma$. In this model TI and TE are determined by inputs to the rhythm generator from the PBN (F_{PBN}), the KF (F_{KF}) and "intrinsic" inputs from other sources (FI), i.e., $T= V_{thresh} /(\Sigma (F_{PBN} +F_{KF}+F_I)$. This model agrees with Butera et al.'s model of the respiratory pacemaker where the activation kinetics of individual respiratory bursting neurons (Butera 1999a) and neuronal populations (Butera 1999b) could be explained solely by persistent sodium leak channel (NaP) and tonic excitatory (tonic-e) inputs (model 1). Baertsch et al. (2018) demonstrated the importance of phasic inhibition for neuronal excitability and thus phase duration, which suggests that Butera's model 2 may be more appropriate where an additional slow leak current results in non-linear changes in conductance and membrane depolarization, analogously to a leaky integrator (fig. 7A).

To calculate F_{PBN} and F_{KF} to phase duration in our *in vivo* model, we assumed that high-volume glutamate injections decreased the activity of these areas to zero, e.g., injection of NBQX and AP5 into the first area (PBN or KF) reduced the contribution of this area (F1) to zero. Subsequent injection into the second area (KF or PBN) reduced the contribution of that area (F2) to zero. This allowed the following calculations: When V_{thresh} =1,

$$T_{control} = 1/(F1 + F2 + F_I) \qquad F1 = (1/T_{control} - 1/T1)$$

$$T1 = 1/(F2 + F_I); F1 = 0 \qquad F2 = (1/T1 - 1/T2)$$

$$T2 = 1/(F_I); F1 = F2 = 0 \qquad F_1 = 1/T2$$

Values for F1, F2 and F_I were calculated using the actual TI and TE values at baseline ($T_{control}$) and after antagonist injections into the PBN and KF for each animal (Protocol 2.6).

The slopes of the linear regression lines for the PBN and KF inputs to TI and TE were compared using Z-scores and pooled t-statistics (Matlab, MathWorks, Natick, MA) (3.5.2.). The ratio of TI:TE contributions from PBN and KF was compared with an unpaired t-test (3.5.2.). Differences were considered significant for $p < 0.05$. Values are expressed as mean ± SE.

3. Results

A total of 47 animals was used for the various protocols. Whenever possible, animals were used for more than one sub-study.

3.1. Functional mapping of the pontine respiratory groups with AMPA injection.

Data was pooled from 17 unilateral maps in 11 animals (bilateral maps in 6 animals). We defined the PBN as the area of maximal AMPA-induced tachypnea and the KF as the area of maximal AMPA- induced bradypnea (Fig. 1A). On average, the PBN was located 1.2±0.2 mm caudal to the inferior colliclе, 2.8±0.1 mm lateral to midline and 7.4±0.2mm ventral to dorsal surface (Fig.2, left). Some degree of tachypnea was consistently observed over a range of 1–2mm rostro-caudal, 2–3mm dorso-ventral, and 0.5–1mm medio-lateral. The KF was located 2.1±0.2 mm caudal to the inferior colliclе, 3.7±0.1 mm lateral to midline and 9.0±0.2mm ventral to the dorsal surface. The area was more circumscribed than the PBN, but bradypnea was usually found over an area of 0.47mm rostro-caudal, 1mm dorso-ventral and 0.5mm medio-lateral. PPA was unchanged or increased in the PBN and decreased in the KF (Fig. 2, right). In the PBN, the change in PPA was generally less pronounced than the change in respiratory rate. While the coordinates relative to inferior colliclе and dorso-ventral location showed some variability, likely due to variation in brainstem to micropipette angle and residual amount of the cerebellar peduncle after cerebellectomy, the spatial relationship between PBN and KF was quite consistent. The KF was located on average 1±0.04 mm caudal, 0.9±0.07 mm lateral and 1.6±0.1mm ventral to the PBN. Extracellular neuronal recordings in the PBN area showed only tonically active neurons. Most neurons in the KF had a tonic discharge pattern, but we very occasionally observed inspiratory activity. We consistently recorded a population of expiratory neurons rostral to the KF and lateral and caudal to the PBN. AMPA injection into that area did not cause any change in respiratory rate or PPA suggesting that these neurons were laryngeal premotor neurons.

3.2. Functional differentiation between the Parabrachial Nucleus and Kölliker-Fuse Nucleus area with AMPA injection

The effects of AMPA injection on respiratory parameters were compared for 15 adjacent PBN-KF pairings. The greatest AMPA responses among all coordinates were averaged for both areas. In the PBN, AMPA injection caused an increase in respiratory rate from 41±2 to 61±3 bpm ($p<0.001$), resulting from a shortening in TI (0.67±0.05s vs. 0.52±0.04s, $p=0.002$) and a shortening in TE (0.83±0.07s vs. 0.51±0.04s, $p<0.001$, Fig. 1B, left). In the KF, AMPA injection caused a decrease in respiratory rate from 41±1 to 33±1 bpm ($p<0.001$),

resulting from an increase in TI (0.68±0.05s vs. 0.77±0.07s, p=0.04) and an increase in TE (0.81±0.06s vs. 1.11±0.08s, p<0.001, Fig. 1B, right). The effects on TI and TE were different between PBN and KF at p<0.001.

These effects on respiratory parameters were observed at PCO2 40mmHg. Interestingly, the magnitude of AMPA effects on respiratory rate in the KF was dependent on the PCO2. In a separate group of animals, AMPA injection into the KF at PCO2 40mmHg decreased respiratory rate from 33±1 bpm to 30±1 bpm due to an increase in TE from 0.98±0.04s to 1.25±0.06s (p<0.001, n=10). This was different at PCO2 50mmHg where AMPA injection into the same location did not change respiratory rate or TE (p<0.001 for respiratory rate at PCO2 40 vs. 50mmHg; p=0.005 for TE at PCO2 40 vs. 50mmHg).

3.3. Histology

In ten animals we injected fluorescent microspheres at the end of the NBQX/AP5 injection protocol into the functionally identified PBN and KF (Fig. 3). Co-staining for Nissl substance and tyrosine hydroxylase confirmed that the antagonist injections were placed within the intended targets. The PBN was located 1.3±0.2 mm caudal to the inferior collicle and 2.7±0.8mm lateral from midline, with anatomical localization medial to the superior cerebellar peduncle, and lateral to the Locus Coeruleus TH positive cell group. The KF was located 2.1±0.2 mm caudal to the inferior collicle and 3.3±0.5mm lateral to midline, with anatomical localization lateral and ventral to the superior cerebellar peduncle. The KF was on average 0.7±0.1mm caudal to the PBN. This distance is somewhat smaller than the distance observed *in vivo* during functional identification with AMPA injections, which is likely due to shrinking of the tissue through the fixation process.

3.4. Inhibition of glutamatergic inputs to the Parabrachial Nucleus and Kölliker-Fuse Nucleus

In 11 animals, we injected NBQX followed by AP5 into the PBN and subsequently into the KF. The combined effect was a large decrease in respiratory rate from 38±4 breaths per minute (bpm) to 4±2 bpm (p<0.001, Fig. 4). The decrease in rate was due to a significant increase in TI (0.72±0.04s vs. 16.9± 2.74s, p<0.001) and TE (0.93±0.1s vs. 19.71±3.49s, p<0.001) with each antagonist injection causing an additional increase. However, apnea was never observed. PPA decreased by 16±4% (p<0.001). In three animals, we injected the antagonists into the PBN in reverse order, i.e., AP5 followed by NBQX. The magnitude of change in all respiratory parameters was similar to the effect when NBQX was injected before AP5 (data not shown). Since we had previously made a similar observation in the medullary rhythm generator where the order of AMPA- and NMDA-receptor antagonist injection had made no difference to the relative effect size (Cook-Snyder 2019), we limited our injection protocols for this study to injecting NBQX first.

In a separate set of 10 animals, we injected NBQX and AP5 into the KF followed by injections into the PBN. Again, this resulted in a large decrease in respiratory rate from 32±3 bpm to 2±1 bpm (p<0.001, Fig. 4) that was due to an increase in TI (0.77±0.05s vs. 18.78±3.43s, p<0.001) and TE (1.21±0.13s vs. 23.47±2.98s, p<0.001). PPA decreased by 16±6 % (p=0.004). Again, apnea was not observed. Injection into the second brainstem area

always resulted in additional significant changes (for TI, TE, RR, all $p \leq 0.001$, for PPA 0.015 and 0.033, resp.).

In 15 of these animals, above antagonist protocol was followed by one minute of mild and one minute of severe hypoxia (Fig. 5A). This increased respiratory rate from 2±0 bpm to 9±1 bpm ($p<0.001$) due to a decrease in TI and TE, which was significantly lower than control (33±2 bpm, $p<0.001$, Fig. 5B). PPA was greatly increased (84±4% to 172±12%, $p<0.001$), which was also higher than the control amplitude (100%, $p<0.001$). However, we frequently observed a reduction of this effect suggesting a secondary hypoxic ventilatory decline before the ventilator was turned back on.

Of note, injection of glutamate antagonists into the rostrolateral pons but outside the PBN did not affect respiratory phase timing or PPA (n=2).

3.5. Additional analyses of the antagonist data on respiratory timing

3.5.1. Changes in inspiratory vs. expiratory duration with antagonist injection: Figure 6B presents an example of the increase in TI and TE during sequential injection of NBQX and AP5 into the KF followed by injections into the PBN. While the absolute breath-by-breath increase was different for TI and TE and also depended on the injection site, both phases consistently increased in duration together. Normalization to TI and TE after the second bilateral antagonist injection into the second brainstem area allowed determination of the percent change with each antagonist injection (Fig. 6C+D). There was some variation in the increase in phase duration with each antagonist injection between animals. On average, glutamate antagonist injections into the first location increased TE to ~40% of maximum regardless of whether the injection was into the PBN or KF (p=0.521). There was a greater increase in TI with antagonist injection into the KF compared to the PBN (p=0.019, Mann-Whitney-U test).

3.5.2. Contributions of the PBN and KF towards phase timing: The contribution of F_{PBN} and F_{KF} to TI vs. TE was approximately linear ($r^2=0.86$ and $r^2=0.80$, resp., Fig. 7B), in line with the observation that TI and TE increased together. The slopes of the regression lines were not significantly different. Since the order of injection affected the magnitude of F_{PBN} and F_{KF}, we calculated the TI:TE ratio to determine how much each area contributed to one phase relative to the other (Fig. 7C). F_{PBN} contributed similarly to TI and TE (ratio 1.0±0.1) whereas F_{KF} contributed more to TI than TE (ratio 1.7±0.2, p=0.002, t-test). The contribution of the pontine respiratory group ($F_{PBN} + F_{KF}$) to phase duration was approximately ten times larger than inputs from other sources (F_I) (for TI: 1.28±0.07 vs. 0.12±0.04, $p<0.001$, and for TE: 0.97±0.07 vs. 0.09±0.03, $p<0.001$).

4. Discussion

This study is the first to use sequential microinjections of AMPA- and NMDA antagonists to determine the individual contributions of the functionally identified PBN and KF areas to respiratory phase duration. While KF activity contributed more to TI, both areas had a large impact on TI and TE. Sequential glutamatergic disfacilitation of both areas reduced respiratory rate by >90%, a depression that could be only partially reversed by high levels of

chemodrive. We propose that *in vivo* inputs from the pontine respiratory group to the medullary rhythm generator significantly affect respiratory rate control while inputs from the RTN determine phrenic motor activity (PPA). The significant prolongation of TI and TE in our study suggests that pontine activity promotes inspiratory on- and off-switch.

4.1. Pontine drive to the medullary respiratory rhythm generator

Cohen showed in decerebrate, vagotomized cats that electrical stimulation of the pneumotaxic center, at that time defined as the area in or near the PBN, caused shortening of TE in a more dorsal region and shortening of TI with TE prolongation in a more ventral region (Cohen 1971). He concluded that activity of these areas contributed to excitability of the respiratory system and "promoted the onset of the succeeding phase". Subsequent studies focused on the pulmonary stretch reflex in non-vagotomized animals and found that lesioning of the pneumotaxic center (Feldman and Gautier 1976) or NMDA- receptor inhibition in the KF (Ling 1994) resulted in very prolonged inspiration ("apneusis") that was often only terminated by the next lung inflation. In vagotomized animals, "cold block" of the pneumotaxic region (St. John 1983) or GABAA-receptor mediated inhibition of the KF (Dutschmann 2006) prolonged TI, and although TE appeared to be routinely increased, research mostly focused on the contribution of the KF to inspiratory off-switch (Dutschmann and Dick 2012). The current study used antagonism of the physiologic glutamatergic inputs to the KF and PBN to show that both areas contributed to inspiratory as well as expiratory phase duration, i.e., inspiratory on- and off-switch. Glutamatergic projections have been shown histologically between the PBN/KF and the medullary rhythm generator (Geerling 2017). In our *in vivo* dog model electrical stimulation of the PBN resulted in excitatory inputs in particular to pre-I neurons, other I-neurons and also E-dec (post-I) neurons in the preBötC; inhibitory inputs were observed in particular to expiratory neurons in the Bötzinger region (Zuperku 2019). Direct connections between the KF and respiratory neurons in the medullary pattern generator were also shown by Ezure and Tanaka using antidromic stimulation (Ezure and Tanaka 2006). On the other hand, cross-correlation analysis showed monosynaptic projections between pons and medulla in only 7% of tested neurons (Segers, Shannon, and Lindsey 1985), which may suggest an additional, indirect pathway.

Butera et al. proposed tonic excitatory inputs as determinants of the pacemaker bursting rate (Butera, Rinzel, and Smith 1999a, 1999b). After transection experiments, Smith et al. introduced tonic pontine "drive" to the medullary rhythm generator as an important contributor to the three-phase respiratory oscillator (Smith et al. 2007). They also showed that in the *in situ* preparation block of NaP channels with riluzole did not completely abolish respiratory rhythm emphasizing the importance of tonic excitatory drive for rhythm generation (Smith et al. 2007). The *in vivo* rabbit model highlights the tonic nature of this drive because in contrast to other species like dogs (Zuperku et al. 2015), cats (Segers et al. 2008), and rats (Ezure and Tanaka 2006) the tachypneic and bradypneic areas of the PBN/KF contain practically no neurons with phasic discharge pattern. We conclude that at least in rabbits the "efferent copy "from the medulla to the KF (Dutschmann and Dick 2012) does not play a role in respiratory phase timing.

4.2. Different contributions of the PBN and KF to the inspiratory on- and off-switch

This study aimed to bridge the gap between our own recent studies exploring the PBN (Miller et al. 2017; Zuperku 2017, 2019) and studies focused on the KF (Barnett 2018; Dhingra 2017; Dutschmann and Dick 2012) to establish whether the contributions to respiratory phase timing were area specific. Functional identification of the KF with AMPA injection matched other studies (Levitt 2015; Dutschmann 2006), and postmortem histology confirmed the injection sites. The functionally identified PBN/KF occupied a substantial area within the pons, i.e., respiratory rate changes with AMPA microinjection (70nl) were observed over a range of about 2mm rostro-caudal, 1–1.5mm medio-lateral and 2–3mm dorso-ventral. We used 700-nl boluses of the antagonists NBQX and AP5, which produced an effective concentration over an estimated radius of ~1200μm around the injection site at 3 minutes after end of injection (Cook-Snyder 2019). On average, antagonist injection into both areas was necessary to achieve maximal respiratory rate depression (Fig. 4). This explains why the respiratory rate depression we observed was greater than in studies where only the KF was inhibited (Dutschmann 2006; Jenkin 2017; Silva 2016). It is possible that the increase in respiratory phase duration also depends on the species as in rats even complete lesioning of the parabrachial pons (Morrison, Cravo, and Wilfehrt 1994) or the entire pneumotaxic center (Wang, Fung, and St John 1993) resulted only in an increase in TI and TE of up to 400%. We found that TI increased more with antagonist injection into the KF while TE increased similarly independent of which area was antagonized first. Recently Barnett et al. amended the oscillator model to include specific excitatory drive from the KF to post-I and early-I neurons in the medullary rhythm generator (Barnett 2018). Excitatory inputs from the KF to medullary post-I neurons was also demonstrated by Song et al. (Song, Tin, and Poon 2015). Our current study highlights the magnitude of these inputs, whose block led to a decrease in respiratory rate by >90%. We also confirmed the importance of the PBN and KF for *expiratory* phase duration and suggest that direct inputs from the PBN and KF to pre-I neurons should be included in the rhythm generator model (Fig. 8).

4.3. Difference in effect on respiratory rate and Peak Phrenic Amplitude

Compared to the significant depression of respiratory rate, in our study PPA was not greatly affected by glutamate antagonists in the pontine respiratory group. This is comparable to studies by Jenkin where injection of the GABAA agonist isoguvacine into the KF depressed PPA by <10% in the *in situ* model (Jenkin 2017) and Silva where injection of the GABAA agonist muscimol into the KF depressed integrated diaphragm activity in *in vivo* rats by 30% at 10% CO2, however, activity was still higher than at 4% CO2 (Silva 2016). Hypoxic and hypercapnic chemodrive are relayed through or generated by the RTN (Takakura et al. 2006; Guyenet, Stornetta, and Bayliss 2008). We propose that phrenic activity (PPA) depends to a large part on chemodrive that is projected directly from the RTN to inspiratory neurons in the preBötC and inspiratory premotor and motoneurons in the medulla and spinal cord (Bochorishvili 2012; Cook-Snyder 2019). Respiratory rate, on the other hand, depends on glutamatergic projections from the RTN to the pontine respiratory group (Bochorishvili 2012; Silva 2016) (Fig. 8). This is supported by our observation that after glutamate antagonism in the PBN/KF hypoxia (Fig. 5) increased respiratory rate only to ~25% of pre-antagonist control while PPA was increased to more than 200% of control. Similarly, in an *in vivo* rat model the hypoxia-induced increase in post-I duration was blocked with AP5

injection into the KF, and this was associated with a large decrease in post-I neuronal activity in the Bötzinger Complex (Song, Tin, and Poon 2015). The increase in PPA with hypoxia appeared to be not affected.

4.4. Differential effects of glutamatergic inputs to the KF

We showed that glutamate antagonist injection into the PBN and KF severely reduced respiratory rate, however, AMPA injection into the KF also caused transient bradypnea. A likely explanation is that AMPA injection activated the nasotrigeminal reflex similar to electrical stimulation of the ethmoidal nerve or glutamate injection into the KF, which also resulted in short apnea (Dutschmann and Herbert 1998). Dutschmann and Herbert proposed that stimulation of the KF neurons increased drive in particular to medullary post-I neurons, resulting in apnea. Neurons appeared to be inhibited by GABAA-ergic inhibition as apnea was longer when inhibition in the KF was blocked with bicuculline (Dutschmann 1998). Interestingly, in our study bradypnea was no longer observed at PCO2 ~50mmHg (see 3.3.) suggesting that increased chemodrive either increased inhibition of these KF neurons or that the concomitantly increased drive to all other medullary rhythm generating neurons was sufficient to balance the additional post-I activity and maintain a regular respiratory rhythm.

4.5. The PBN/KF as a potential target for respiratory stimulating drugs

Respiratory rate depression by opioids and other sedative drugs has become an increasing threat to public health (Clinton 2019), and many studies have investigated drugs that increase respiratory rate through their effect on the preBötC (Manzke et al. 2003; Guenther et al. 2012; Ren et al. 2009). However, none of these drugs was effective to overcome opioid-induced respiratory depression at analgesic opioid levels in humans (review in (Dahan 2018)). We have previously shown in non-vagotomized, decerebrate rabbits that opioid-induced respiratory rate depression at clinical dose-rates of remifentanil can be partially antagonized in the PBN (Miller et al. 2017). Given the significant role of the pontine respiratory group in respiratory rate control that we observed, it may be most effective to pursue drugs that increase activity of the PBN/KF and thus increase drive to the phase-switching neurons of the medullary rhythm generator. While the importance of NMDA-receptor mediated drive to the PBN/KF has been well described (Song, Tin, and Poon 2015), this is the first study to show that AMPA receptors, too, mediate a substantial portion of the glutamatergic inputs. Both receptor subtypes may be suitable targets for respiratory stimulating drugs.

4.5. Methodological considerations

4.5.1. Effects of hypercapnia and hypoxia: Our antagonist injection protocols were performed at a PCO2 ~50mmHg to match previous studies from our laboratory that investigated the effects of opioids on the PBN (Miller et al. 2017) and preBötC (Stucke et al. 2015). We found that this CO2 level confounded physiologic reflexes like the trigeminal ethmoidal reflex (Dutschmann and Herbert 1998), i.e., only minimal bradypnea was observed with AMPA injection into the KF at PCO2≥50 mmHg. We thus used PCO2≤40mmHg until the KF was identified bilaterally and then increased the PCO2 for the antagonist injection protocols.

Hypercapnia did not prevent the significant decrease in respiratory rate with glutamate antagonist injection. Peak respiratory rate of the CO2 response curve in the decerebrate rabbit preparation is reached around 65mmHg (unpublished data, AGS, 2008). In four animals in the current study, etCO2 was 60±2mmHg before the hypoxic response trial, however, the respiratory rate in these animals (2±0.2 bpm) was not different from the respiratory rate in all animals (2.0±0bpm, average etCO2 49±2mmHg). This suggests that the increase in respiratory rate to 9±2bpm during paused ventilation was mostly due to hypoxia and not to any additional increase in PCO2 (65±4mmHg).

4.5.2. Localization of the PBN and KF with AMPA injection: Similar to previous studies using glutamate injections in rats (Chamberlin and Saper 1994) or DLH injections in rabbits (Mutolo et al. 1998) we found that AMPA injections into the rostral pons elicited tachypnea or bradypnea over an area of several millimeters. There was significant overlap between response types in other studies, which may have resulted from summarizing the responses at each stereotaxic coordinate from all animals. In contrast, we rarely observed tachypnea and bradypnea at the same rostro-caudal level within one animal and we found that in individual animals the area of *maximal* tachypnea (PBN) was consistently located rostral and medial to the area of *maximal* bradypnea (KF) (Fig. 2).

Histologically, injection sites were located within or near the outlines of the medial and lateral PBN and KF (Meessen 1949). Overall, identification of the “PBN” matched the “tachypneic area of the PBN” in our earlier study (Miller et al. 2017) although the present histology suggested that the response was not limited to the medial PBN. Recent publications showing a wide distribution of, e.g., glutamatergic, GABAergic and FoxP2 positive neurons in the rostral pons (Geerling 2017; Stanic 2018) raise the question whether the superimposed areas in the traditional atlas adequately reflect respiratory neuronal populations of the same function.

Despite consistency in the AMPA mapping, the magnitude of the glutamate antagonist effects with each injection could vary substantially (Fig. 6A, C+D). In a few animals, maximal respiratory rate depression was achieved with injections solely into the PBN or KF, however, in most animals injections into both locations were necessary to achieve full effect. We have estimated that NBQX and AP5 injections (700nl) reach an effective concentration with a radius of 1000–1200μm within ~3 minutes (Cook-Snyder 2019). This emphasizes that the neuronal population of interest lies within a spherical diameter of more than 2 mm. We conclude that AMPA injections (70nl, radius~400–500μm)(Cook-Snyder 2019) provide only approximate markers of the entire neuronal population, however, the prominent respiratory rate depression when antagonists were injected into the functionally identified PBN *and* KF suggests that in combination these markers can capture the full extent of the respiratory rate controlling neurons in the PBN/KF.

5. Conclusion

We showed in an adult, *in vivo* decerebrate rabbit model that tonic drive from the PBN/KF area was a major determinant of inspiratory and expiratory phase duration. Peak phrenic activity was much less affected. The importance of the pontine respiratory group for

respiratory rate control makes it a good target for the development of drugs that can increase respiratory rate during opioid-induced respiratory depression.

Acknowledgements

The authors thank Jack Tomlinson (Biologic Laboratory Technician) for excellent technical assistance and Andrew Williams (Engineering Technician) for his outstanding support with the experimental setup (both Medical College of Wisconsin, Milwaukee, Wisconsin).

This work was supported by the NIH (RO1-GM112960, Dr. Stucke) and VA merit award (I01BX000721, Dr. Zuperku).

References

Barnett WM, Jenkin SEM, Milsom WK, Paton JFR, Abdala AP, Molkov YI, Zoccal DB. 2018 ‘The Kölliker- Fuse nucleus orchestrates the timing of expiratory abdominal nerve bursting’, J Neurophysiol, 119: 401–12. [PubMed: 29070631]

Bochorishvili G.Stornetta RL, Coates MB, Guyenet PG. 2012 ‘Pre-Bötzinger complex receives glutamatergic innervation from galaninergic and other retrotrapezoid nucleus neurons.’, J Comp Neurol, 520: 1047–61. [PubMed: 21935944]

Butera RJ Jr., Rinzel J, and Smith JC. 1999a ‘Models of respiratory rhythm generation in the pre-Bötzinger complex. I. bursting pacemaker neurons’, J. Neurophysiol., 81: 382–97.

Butera RJ Jr., Rinzel J, and Smith JC. 1999b ‘Models of respiratory rhythm generation in the pre-Bötzinger complex. II. populations of coupled pacemaker neurons’, J. Neurophysiol., 81: 398–415.

Chamberlin NL, and Saper CB. 1992 ‘Topographic organization of cardiovascular responses to electrical and glutamate microstimulation of the parabrachial nucleus in the rat’, J Comp Neurol, 326: 245–62. [PubMed: 1362207]

Chamberlin NL, and Saper CB. 1994 ‘Topographic organization of respiratory responses to glutamate microstimulation of the parabrachial nucleus in the rat’, J Neurosci, 14: 6500–10. [PubMed: 7965054]

Clinton HA, Hunter AA, Logan SB, Lapidus GD. 2019 ‘Evaluating opioid overdose using the National Violent Death Reporting System, 2016’, Drug Alcohol Depend, 194: 371–6. [PubMed: 30481691]

Cohen MI 1971 ‘Switching of the respiratory phases and evoked phrenic responses produced by rostral pontine electrical stimulation.’, J.Physiol.(London), 217: 133–58. [PubMed: 5571915]

Cook-Snyder DR, Miller JR, Navarrete-Opazo AA, Callison JJ, Peterson RC, Hopp FA, Stuth EA, Zuperku EJ, Stucke AG. 2019 ‘The contribution of endogenous glutamatergic input in the ventral respiratory column to respiratory rhythm’, Respir Physiol Neurobiol, 260: 37–52. [PubMed: 30502519]

Cui Y, Kam K, Sherman D, Janczewski WA, Zheng Y, Feldman JL. 2016 ‘Defining preBötzinger Complex rhythm- and pattern-generating neural microcircuits in vivo’, Neuron, 91: 602–14. [PubMed: 27497222]

Dahan A, van der Schrier R, Smith T, Aarts L, van Velzen M, Niesters M 2018 ‘Averting opioid-induced respiratory depression without affecting anesthesia’, Anesthesiology, 128: 1027–37. [PubMed: 29553984]

Del Negro CA, Funk GD, Feldman JL. 2018 ‘Breathing matters’, Nat Rev Neurosci, 19: 351–67. [PubMed: 29740175]

Dhingra RR, Dutschmann M, Galan RF, Dick TE. 2017 ‘Kölliker-Fuse nuclei regulate respiratory rhythm variability via a gain-control mechanism’, Am J Physiol Regul Integr Comp Physiol, 302: R172–R88.

Dogas Z, Krolo M, Stuth EA, Tonkovic-Capin M, Hopp FA, McCrimmon DR, and Zuperku EJ. 1998 ‘Differential effects of GABAA receptor antagonists in the control of respiratory neuronal discharge patterns’, J Neurophysiol, 80: 2368–77. [PubMed: 9819249]

Dutschmann M, Herbert H 2006 ‘The Kolliker-Fuse nucleus gates the postinspiratory phase of the respiratory cycle to control inspiratory off-switch and upper airway resistance in rat’, Eur J Neurosci, 24: 1071–84. [PubMed: 16930433]

Dutschmann M, Morschel M,, Reuter J, Zhang W, Gestreau C, Stettner GM, and Kron M. 2008 ‘Postnatal emergence of synaptic plasticity associated with dynamic adaptation of the respiratory motor pattern’, Respiratory Physiology & Neurobiology, 164: 72–9. [PubMed: 18620081]

Dutschmann M, and Dick TE. 2012 ‘Pontine mechanisms of respiratory control’, Compr Physiol, 2: 2443–69. [PubMed: 23720253]

Dutschmann M, and Herbert H. 1998 ‘NMDA and GABAA receptors in the rat Kolliker-Fuse area control cardiorespiratory responses evoked by trigeminal ethmoidal nerve stimulation’, J Physiol, 510 (Pt 3): 793–804. [PubMed: 9660894]

Eldridge FL 1976 ‘Expiratory effects of brief carotid sinus nerve and carotid body stimulations’, Respir.Physiol., 26: 395–410. [PubMed: 951542]

Ezure K 1990 ‘Synaptic connections between medullary respiratory neurons and considerations on the genesis of respiratory rhythm’, Progress in Neurobiology, 35: 429–50. [PubMed: 2175923]

Ezure K, and Tanaka I. 2006 ‘Distribution and medullary projection of respiratory neurons in the dorsolateral pons of the rat’, Neuroscience, 141: 1011–23. [PubMed: 16725272]

Feldman JL, and Gautier H. 1976 ‘Interaction of pulmonary afferents and pneumotaxic center in control of respiratory pattern in cats’, J.Neurophysiol, 39: 31–44. [PubMed: 1249602]

Geerling JC, Yokota S, Rukhadze I, Roe D, Chamberlin NL. 2017 ‘Kölliker-Fuse GABAergic and glutamatergic neurons project to distinct targets.’, J Comp Neurol, 525: 1844–60. [PubMed: 28032634]

Guenther U, Theuerkauf NU, Huse D, Boettcher MF, Wensing G, Putensen C, and Hoeft A. 2012 ‘Selective 5-HT(1A)-R-agonist repinotan prevents remifentanil-induced ventilatory depression and prolongs antinociception’, Anesthesiology, 116: 56–64. [PubMed: 22082683]

Guyenet PG, Stornetta RL, and Bayliss DA. 2008 ‘Retrotrapezoid nucleus and central chemoreception’, J Physiol, 586: 2043–8. [PubMed: 18308822]

Jenkin SE, Milsom WK, Zoccal DB. 2017 ‘The Kölliker-Fuse nucleus acts as a timekeeper for late-expiratory abdominal activity’, Neuroscience, 348: 63–72. [PubMed: 28188852]

Kam K, Worrell JW, Janczewski WA, Cui Y, and Feldman JL. 2013 ‘Distinct inspiratory rhythm and pattern generating mechanisms in the preBotzinger complex’, J Neurosci, 33: 9235–45. [PubMed: 23719793]

Krolo M, Stuth EA, Tonkovic-Capin M, Dogas Z, Hopp FA, McCrimmon DR, and Zuperku EJ. 1999 ‘Differential roles of ionotropic glutamate receptors in canine medullary inspiratory neurons of the ventral respiratory group’, J Neurophysiol, 82: 60–8. [PubMed: 10400935]

Levitt ES, Abdala AP, Paton JFR, Bissonnette JM, Williams JT. 2015 ‘Mu-opioid receptor activation hyperpolarizes respiratory-controlling Kölliker-Fuse neurons and suppresses post-inspiratory drive’, J Physiol, 593: 4453–69. [PubMed: 26175072]

Ling L, Karius DR, Speck DF. 1994 ‘Role of N-methyl-D-aspartate receptors in the pontine pneumotaxic mechanism in the cat’, J.Appl.Physiol., 76(3): 1138–43. [PubMed: 8005856]

Manzke T, Guenther U, Ponimaskin EG, Haller M, Dutschmann M, Schwarzacher S, and Richter DW. 2003 ‘5-HT4(a) receptors avert opioid-induced breathing depression without loss of analgesia’, Science, 301: 226–9. [PubMed: 12855812]

Meessen H, Olszewski J 1949 Cytoarchitectonischer Atlas des Rautenhirns des Kaninchens (Karger: Basel).

Miller JR, Zuperku EJ, Stuth EAE, Banerjee A, Hopp FA, and Stucke AG. 2017 ‘A Subregion of the Parabrachial Nucleus Partially Mediates Respiratory Rate Depression from Intravenous Remifentanil in Young and Adult Rabbits’, Anesthesiology, 127: 502–14. [PubMed: 28590302]

Molkov YI, Rubin JE, Rybak IA, Smith JC. 2017 ‘Computational models of the neural control of breathing’, Wiley Interdiscip Rev Syst Biol Med, 9: doi: 10.1002/wsbm.371.

Morgado-Valle C, and Feldman JL. 2007 ‘NMDA receptors in preBotzinger complex neurons can drive respiratory rhythm independent of AMPA receptors’, J Physiol, 582: 359–68. [PubMed: 17446224]

Morrison SF, Cravo SL, and Wilfehrt HM. 1994 'Pontine lesions produce apneusis in the rat', Brain Res, 652: 83–6. [PubMed: 7953724]

Mutolo D, Bongianni F, Carfi M, and Pantaleo T. 1998 'Respiratory responses to chemical stimulation of the parabrachial nuclear complex in the rabbit', Brain Res, 807: 182–6. [PubMed: 9757031]

Mutolo D, Bongianni F, Nardone F, and Pantaleo T. 2005 'Respiratory responses evoked by blockades of ionotropic glutamate receptors within the Botzinger complex and the pre-Botzinger complex of the rabbit', Eur J Neurosci, 21: 122–34. [PubMed: 15654849]

Prkic I, Mustapic S, Radocaj T, Stucke AG, Stuth EA, Hopp FA, Dean C, and Zuperku EJ. 2012 'Pontine mu-opioid receptors mediate bradypnea caused by intravenous remifentanil infusions at clinically relevant concentrations in dogs', J Neurophysiol, 108: 2430–41. [PubMed: 22875901]

Ren J, X Ding GD Funk, and Greer JJ. 2009 'Ampakine CX717 protects against fentanyl-induced respiratory depression and lethal apnea in rats', Anesthesiology, 110: 1364–70. [PubMed: 19461299]

Segers LS, Nuding SC, Dick TE, Shannon R, Baekey DM, Solomon IC, Morris KF, and Lindsey BG. 2008 'Functional connectivity in the pontomedullary respiratory network', J Neurophysiol, 100: 1749–69. [PubMed: 18632881]

Segers LS, Shannon R, and Lindsey BG. 1985 'Interactions between rostral pontine and ventral medullary respiratory neurons', J Neurophysiol, 54: 318–34. [PubMed: 4031991]

Silva JN, Lucena EV, Silva TM, Damasceno RS, Takakura AC, Moreira TS. 2016 'Inhibition of the pontine Kölliker-Fuse nucleus reduces genioglssal activity elicited by stimulation of the retrotrapezoid chemoreceptor neurons', Neuroscience, 328: 9–21. [PubMed: 27126558]

Smith JC, Abdala AP, Koizumi H, Rybak IA, and Paton JF. 2007 'Spatial and functional architecture of the mammalian brain stem respiratory network: a hierarchy of three oscillatory mechanisms', J Neurophysiol, 98: 3370–87. [PubMed: 17913982]

Song G, Tin C, and Poon CS. 2015 'Multiscale fingerprinting of neuronal functional connectivity', Brain Struct Funct, 220: 2967–82. [PubMed: 25056933]

St. John WM, Bianchi AL. 1983 'Comparison of activities of medullary respiratory neurons in eupnea and apneusis', Respir Physiol, 51: 361–77. [PubMed: 6844766]

Stanic D, Dhingra RR, Dutschmann M 2018 'Expression of the transcription factor FOXP2 in brainstem respiratory circuits of adult rat is restricted to upper-airway pre-motor areas.', Respir Physiol Neurobiol, 250: 14–8. [PubMed: 29414420]

Stucke AG, Miller JR, Prkic I, Zuperku EJ, Hopp FA, and Stuth EA. 2015 'Opioid-induced Respiratory Depression Is Only Partially Mediated by the preBotzinger Complex in Young and Adult Rabbits In Vivo', Anesthesiology, 122: 1288–98. [PubMed: 25751234]

Takakura AC, Moreira TS, Colombari E, West GH, Stornetta RL, and Guyenet PG. 2006 'Peripheral chemoreceptor inputs to retrotrapezoid nucleus (RTN) CO2-sensitive neurons in rats', J Physiol, 572: 503–23. [PubMed: 16455687]

Wang W, Fung ML, and St John WM. 1993 'Pontile regulation of ventilatory activity in the adult rat',Journal of Applied Physiology, 74: 2801–11. [PubMed: 8365984]

Zuperku EJ, Prkic I, Stucke AG, Miller JR, Hopp FA, and Stuth EA. 2015 'Automatic classification of canine PRG neuronal discharge patterns using K-means clustering', Respir Physiol Neurobiol, 207: 28–39. [PubMed: 25511381]

Zuperku EJ, Stucke AG, Hopp FA, and Stuth EA. 2017 'Characteristics of breathing rate control mediated by a subregion within the pontine parabrachial complex', J Neurophysiol, 117: 1030–42. [PubMed: 27974449]

Zuperku EJ, Stucke AG, Hopp FA, Stuth EA. 2017 'Characteristics of breathing rate control mediated by a subregion within the pontine parabrachial complex.', J Neurophysiol, 117: 1030–42. [PubMed: 27974449]

Zuperku EJ, Stucke AG, Krolikowski JG, Tomlinson J, Hopp FA, Stuth EA. 2019 'Inputs to medullary respiratory neurons from a pontine subregion that controls breathing frequency', Respir Physiol Neurobiol, 265: 127–40. [PubMed: 29964165]

Highlights

- Glutamatergic input to the Parabrachial Nucleus/ Kolliker---Fuse determines respiratory rate.
- The Parabrachial Nucleus and Kolliker---Fuse contribute to in--- and expiratory phase duration.
- The Parabrachial Nucleus/ Kolliker---Fuse contribute only little to peak phrenic amplitude.

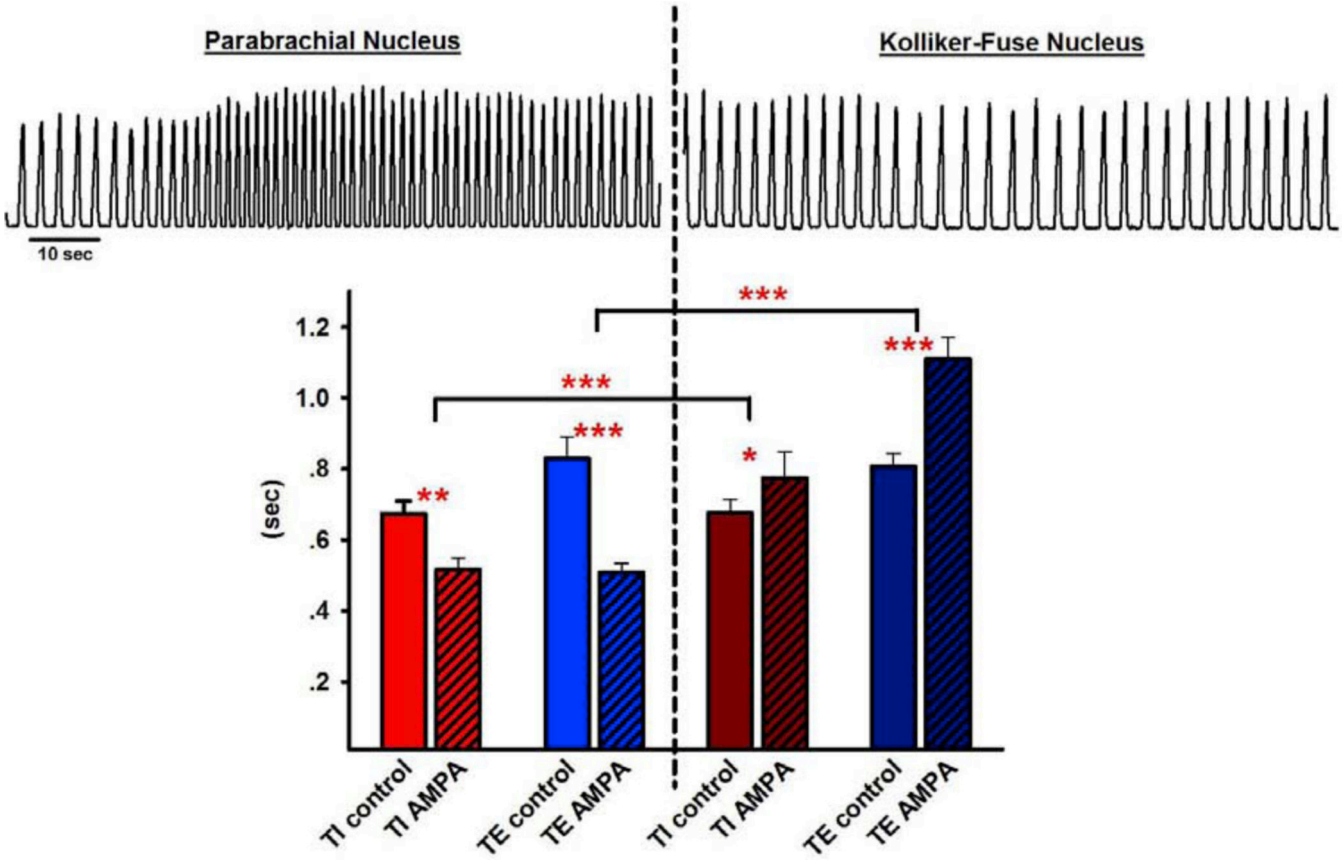

Figure 1,

upper: Phrenic neurogram (arbitrary units) tracings before and after injection of AMPA (50μM, 70nl) into the Parabrachial Nucleus (PBN, left) and adjacent Kölliker-Fuse Nucleus (KF, right). **Lower:** Pooled data from 15 injections into adjacent PBN - KF pairs showed that AMPA decreased inspiratory (TI) and expiratory (TE) duration in the PBN while it increased both phases in the KF. 2-way RM ANOVA, factors: injections site, drug. *p<0.05, **p<0.01, ***: p<0.001.

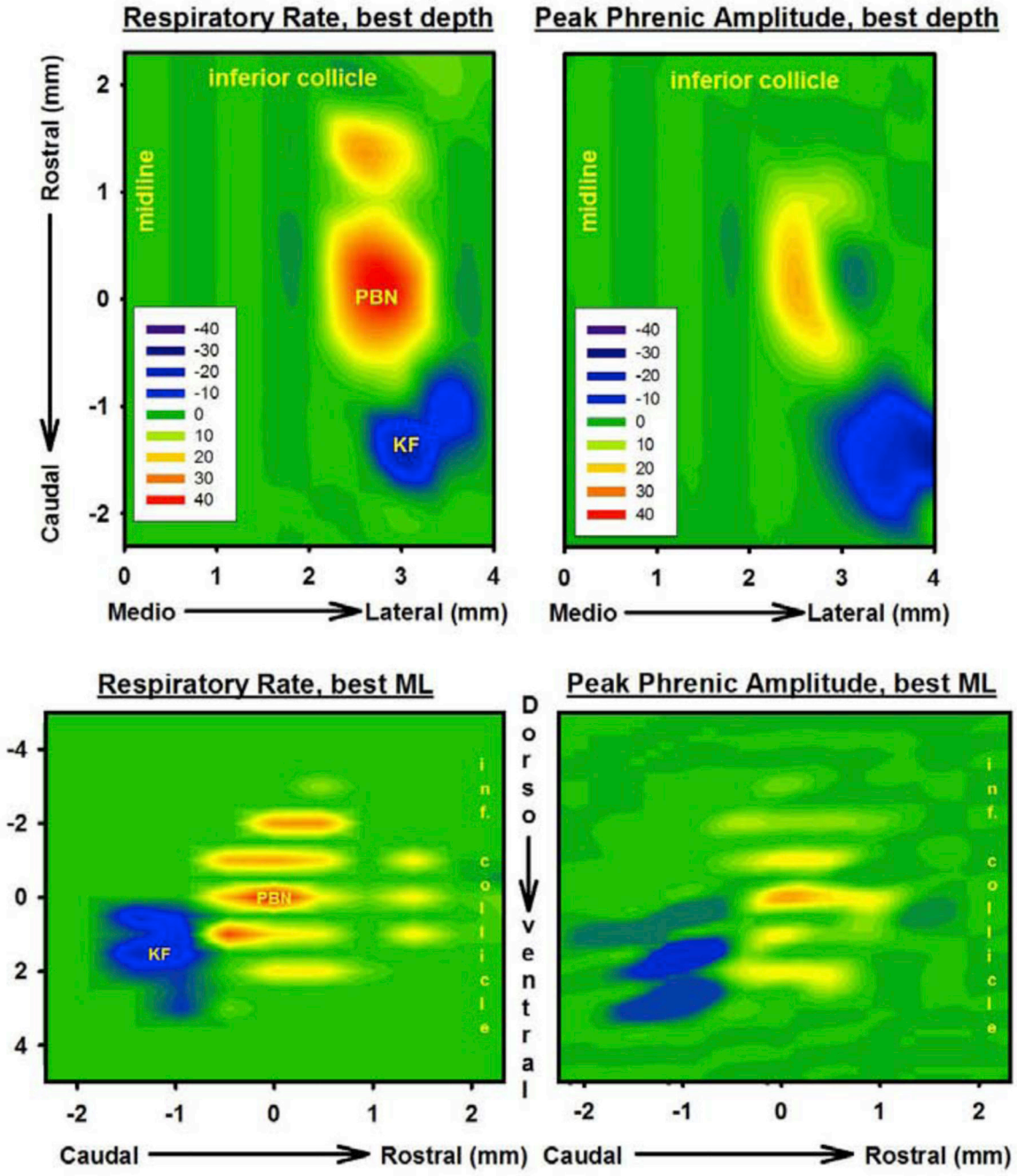

Figure 2:

Contour plots from 10 gridwise injections (step 0.5mm) of AMPA (50μM, 70nl) indicate percent changes from baseline, plotted for respiratory rate (left) and peak phrenic activity (right). **Upper:** Plots depict the greatest change at any dorso-ventral coordinate. Medio-lateral (M/L) coordinates are relative to midline. The coordinate where AMPA injection caused maximal tachypnea was labeled the Parabrachial Nucleus (PBN). The area of maximal bradypnea was labeled the Kölliker-Fuse Nucleus (KF). Rostro-caudal coordinates are relative to the PBN (PBN = 0). **Lower:** Plots depict the greatest change at any medio-

lateral coordinate. Dorso-ventral coordinates are relative to the PBN (PBN=0). Note that for clarity only those animals were included where the KF was 1mm caudal and 0.5mm lateral to the PBN. Inclusion of animals where the KF was 0.5mm caudal or 1mm lateral from the PBN would have overestimated the dimensions of both areas. Average values for the location of PBN and KF in the text (3.1.) include all coordinates. Scale: ≥+40% (red) to −40% (blue) from baseline, green: no change.

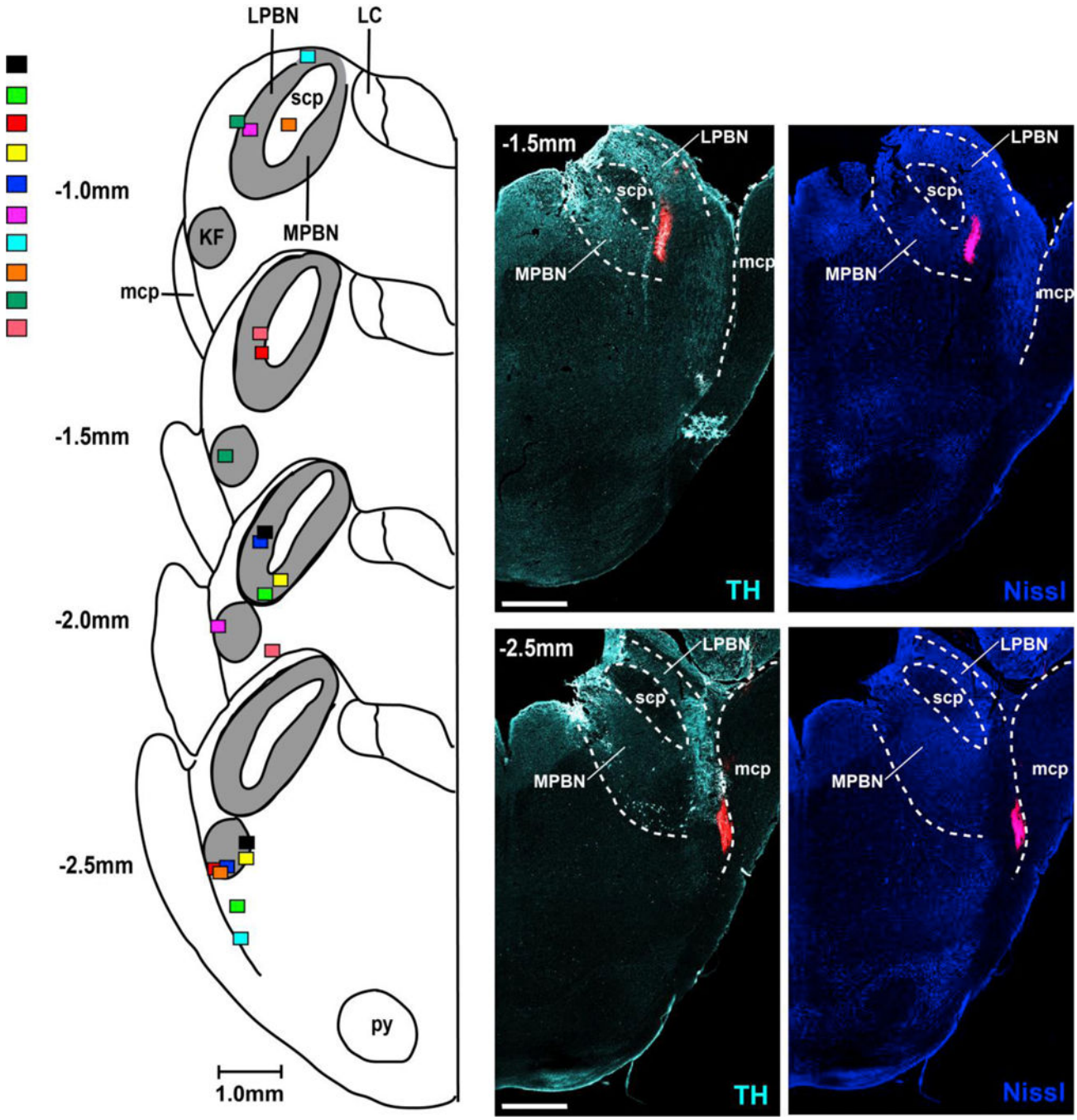

Figure 3:

Injections of fluorescent latex microspheres (Retrobeads, Lumiflor Inc., 5%, 140nl) confirm the location of the Parabrachial Nucleus (PBN) and Kölliker-Fuse (KF). Left: Diagrammatic hemisections of the pons at each rostro-caudal level with the individual injection sites superimposed, each color representing one animal. The rostro-caudal distance between the PBN and KF within the same animal was on average 1mm. Right: Corresponding hemisections from one animal with immunoreactivity for tyrosine hydroxylase (TH, left) and Nissl substance (right). LPBN: lateral Parabrachial Nucleus; scp: superior cerebellar

peduncle; MPBN: medial Parabrachial Nucleus; mcp: medial cerebellar peduncle. Bar=1mm.

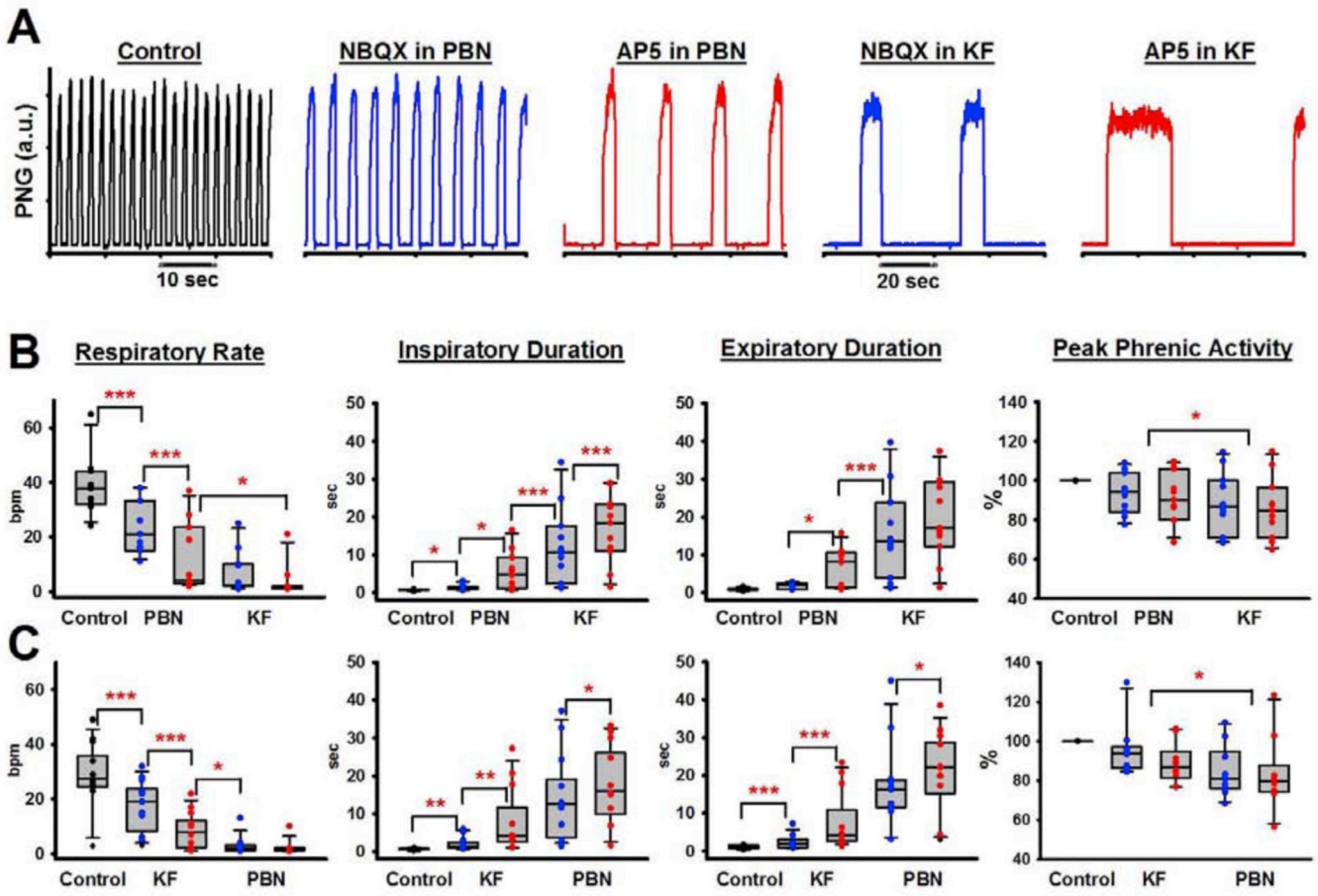

Figure 4:

A: Phrenic neurogram showing the effect of bilateral injection of the AMPA receptor antagonist NBQX followed by the NMDA receptor antagonist AP5 into the functionally identified Parabrachial Nucleus (PBN) and then Kölliker-Fuse Nucleus (KF) in one adult rabbit. **B:** Pooled data of the effect of NBQX (blue) and AP5 (red) injection into the PBN, followed by the KF (n=11). **C:** Pooled data of the effect of NBQX and AP5 injection into the KF, followed by the PBN in 10 different rabbits. 2-way RM ANOVA with factors: injection site, drug. Asterisks refer to the comparisons between drug injections as indicated by brackets. *p<0.05, **p<0.01, ***p<0.001.

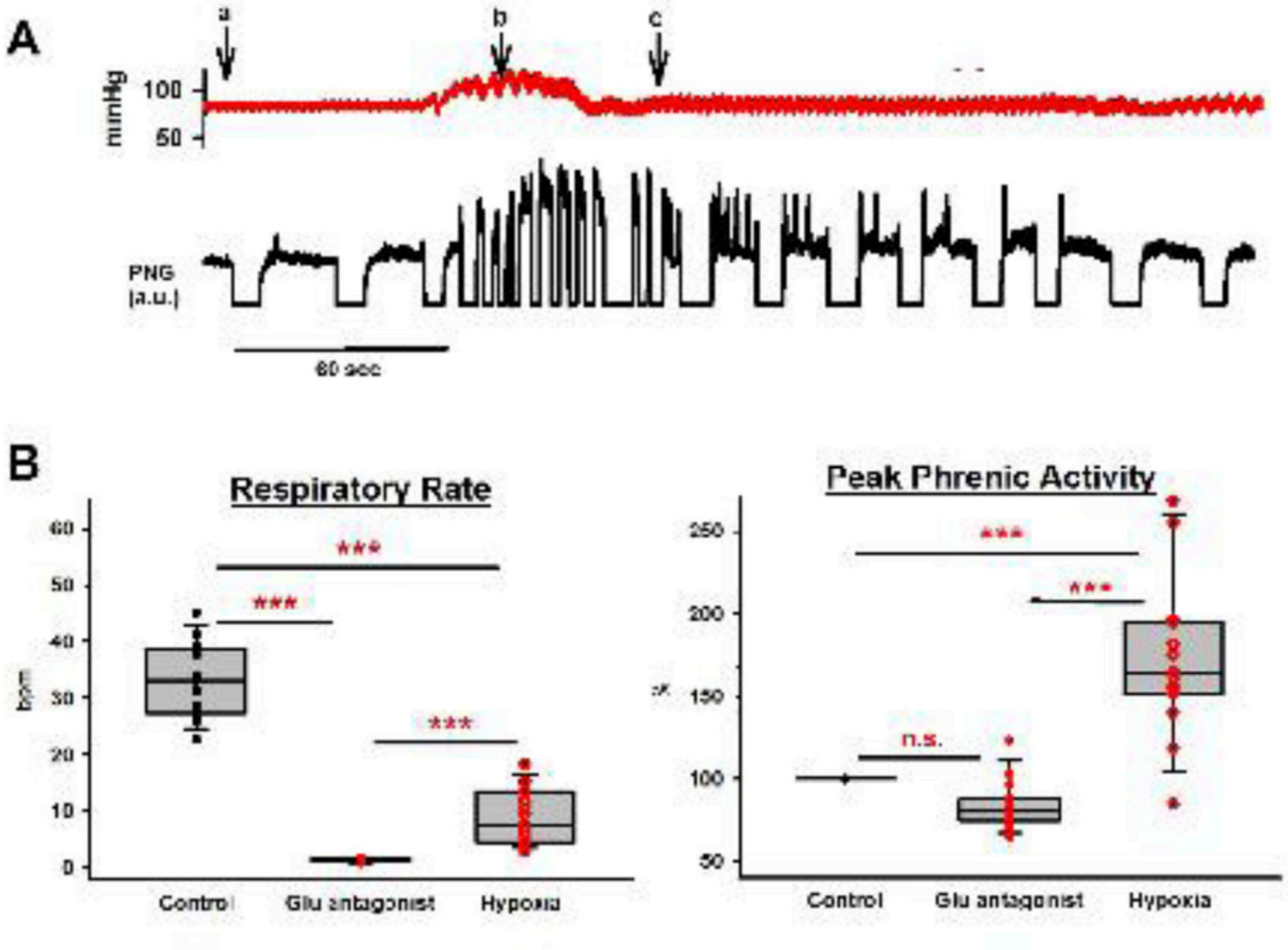

Figure 5:

A: Arterial blood pressure tracings and phrenic neurogram (PNG, arbitrary units) during exposure to hypoxia following glutamate antagonist injection into the Parabrachial Nucleus and Kölliker-Fuse Nucleus. **a:** FiO2 0.17, expiratory CO2 50mmHg, **b:** stopping ventilator, **c:** restarting ventilator. Mild hypoxia (FiO2 0.17) already led to an increase in blood pressure and peak phrenic activity (PPA). Secondary hypoxic ventilatory decline of PPA and respiratory rate already began before the ventilator was restarted. Gasping activity on top of the apneustic pattern was frequently observed during the first breaths after restarting the ventilator. **B:** Pooled data for 15 animals showed that hypoxia only partially reversed the depression of respiratory rate when pontine activity was eliminated through glutamate (Glu) antagonist injection. In contrast, PPA was increased significantly above control levels.

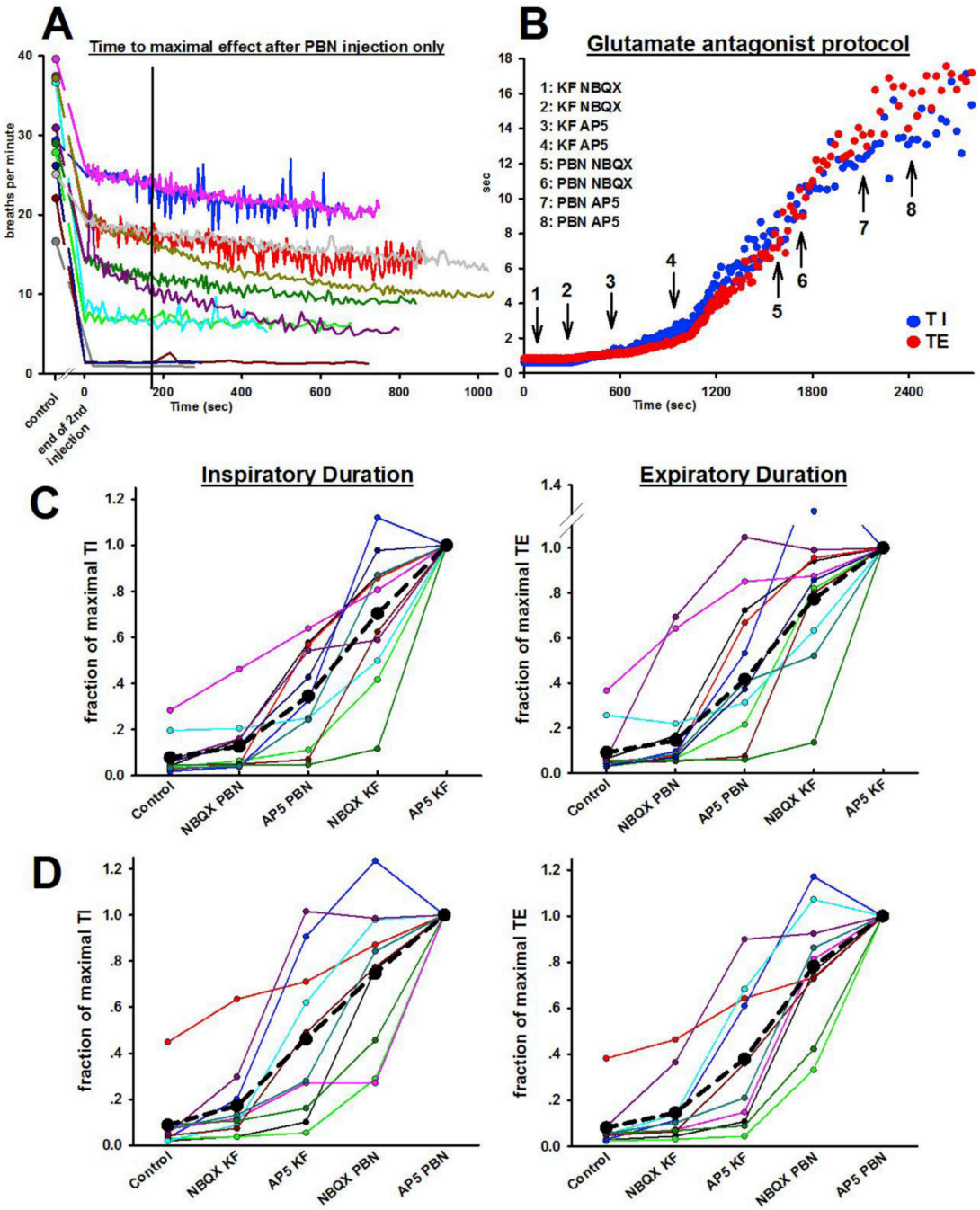

Figure 6:

A: Pilot study to determine the time course of the change in respiratory rate after bilateral injection of the AMPA receptor antagonist NBQX followed by the NMDA receptor antagonist AP5 into the functionally identified Parabrachial Nucleus (PBN)(n= 12). In all animals, respiratory rate had decreased significantly from the control rate (circle) to the end of the AP5 injection (Time 0 seconds). In most animals, the decrease in respiratory rate plateaued ~3 minutes after the end of the AP5 injection (black line) or continued to further decrease only minimally. **B:** Representative example from one animal of the increase in

inspiratory (TI) and expiratory (TE) duration with bilateral injections of NBQX and AP5, first into the bilateral KF and then into the bilateral PBN. **C+D:** Changes in TI (left) and TE (right) with each antagonist injection, relative to the maximal value for TI and TE after the last injection. Each color represents one animal. While there is variation between the effect size of each injection, the average (black dotted line) suggest that both receptor subtypes in both areas contribute to phase duration in an additive fashion. B: Injection order PBN, then KF, n=11. C: Injection order KF, then PBN, n=10.

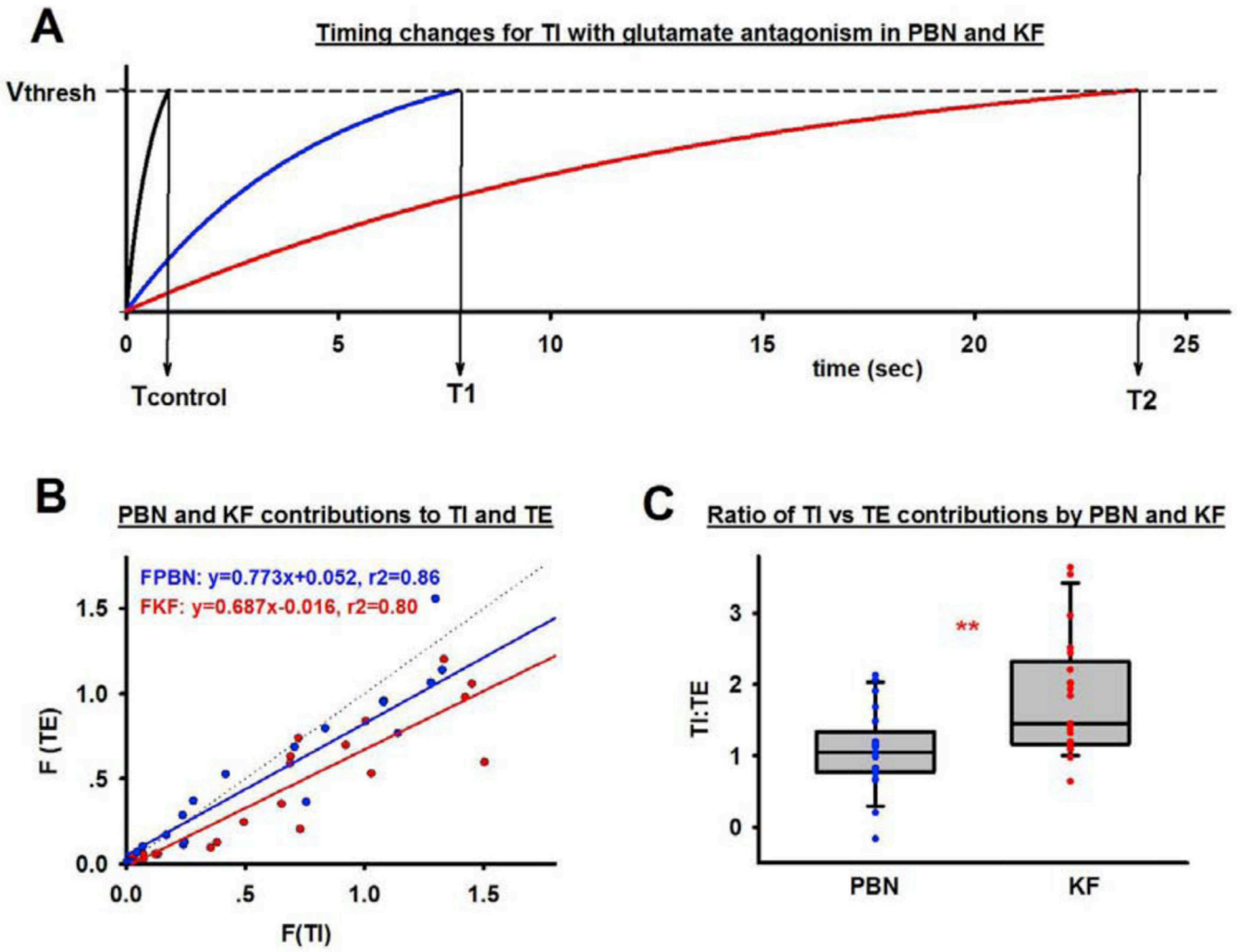

Figure 7:

A: Respiratory phase timing can be modeled in analogy to a "leaky integrator" where the sum of inputs determines phase duration T according to $\mathbf{T = V_{threshold}/\Sigma(\ inputs)}$ See text (3.5.2.) for details. This example used the average values for inspiratory duration at control (black) and after NBQX and AP5 injection into the Kölliker-Fuse Nucleus (KF, blue) and Parabrachial Nucleus (PBN, red). Glutamate antagonist injection reduced KF inputs to the rhythm generator to 0, which decreased the sum of inputs, the threshold was reached later and the phase time (T1) was longer. After subsequent antagonist injection into the PBN phase switch solely depended on inputs to the rhythm generator from outside the pons, resulting in a very long TI. **B:** Inputs (F) to inspiratory (TI) versus expiratory (TE) duration are plotted for the PBN (blue) and KF (red) without regard to injection order (n=21). Inputs follow a linear distribution. **C:** Ratio of glutamatergic inputs to TI and TE from the PBN (blue) and KF (red) for 21 animals. The KF contributed more to TI than to TE, while the PBN contributed evenly to both phase durations. **: $p<0.01$.

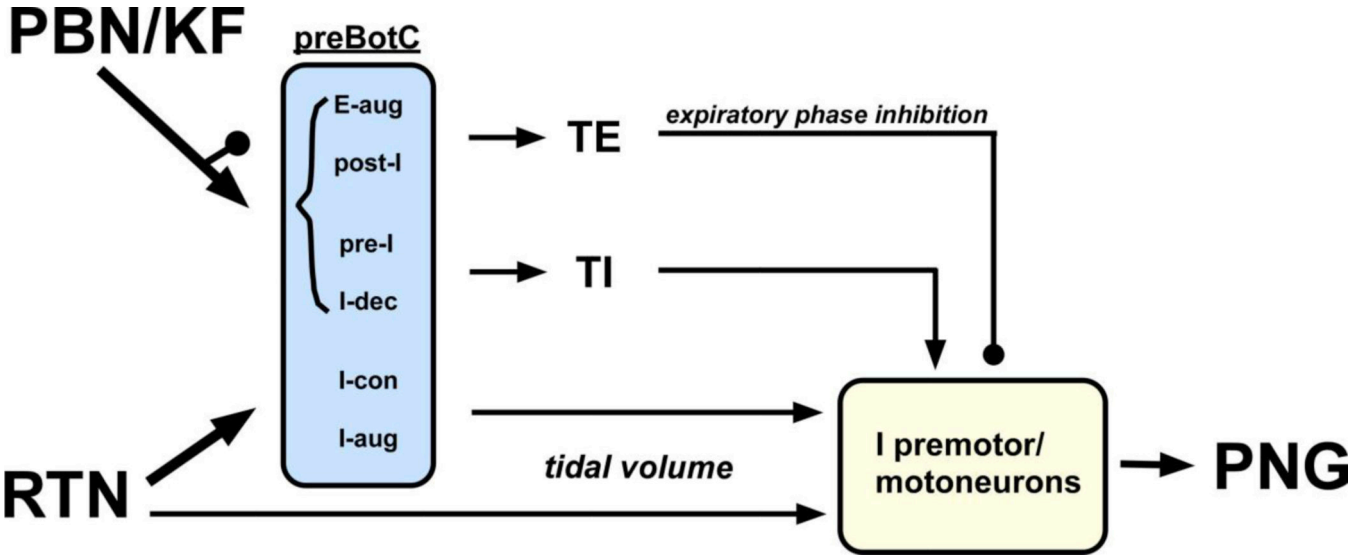

Figure 8:

Schematic of Parabrachial Nucleus/ Kölliker-Fuse (PBN/KF) and Retrotrapezoid Nucleus (RTN) contributions to phrenic nerve activity (PNG). Pontine nuclei greatly contribute to respiratory rate by providing excitatory and inhibitory inputs to the phase-switch neurons in the preBötzinger Complex (preBötC) while RTN input determines respiratory motor output through excitatory drive to inspiratory (I) preBötC, premotor and motoneurons. Minor contributions from the pons to tidal volume and from the RTN towards phase-switch are not depicted. Neuron types in the rhythm generator are adapted from Barnett et al. (2018) and Zuperku et al. (2019). See text (4.2. and 4.3.) for details. E-aug: expiratory augmenting; E-dec: expiratory decrementing; pre-I: pre-inspiratory; I-dec: inspiratory decrementing; I-con: inspiratory constant; I-aug: inspiratory augmenting; TI: inspiratory duration; TE: expiratory duration; arrow: excitatory inputs; button: inhibitory inputs.